Colloids and Surfaces A: Physicochemical and Engineering Aspects 728 (2026) 138807

Contents lists available at ScienceDirect

Colloids and Surfaces A: Physicochemical and Engineering Aspects

journal homepage: www.elsevier.com/locate/colsurfa

In-situ investigation of crack formation during drying of catalyst layers for polymer electrolyte membrane (PEM) fuel cells and electrolyzer

Nadine Zimmerer *, Philipp Quarz, Linus Janning, Philip Scharfer, Wilhelm Schabel

Thin Film Technology (TFT), Karlsruhe Institute of Technology (KIT), Straße am Forum 7, Karlsruhe D-76131, Germany

GRAPHICAL ABSTRACT

The study investigates crack formation in-situ during the drying of catalyst layers for PEM fuel cells and electrolyzers using different camera systems. The rise in film temperature during drying is identified as the critical point for crack initiation. Theoretical considerations on selective drying complement the experimental findings on the drying and cracking behavior of different ink formulations.

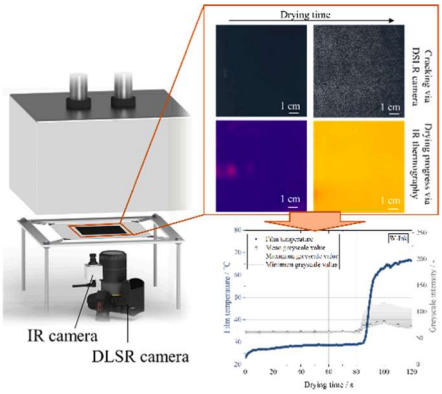

ARTICLE INFO

Keywords:
Cracking
Ink drying
Ink composition
PEM fuel cells and electrolyzers
Arheotrope
Selective drying

ABSTRACT

The formation of cracks in catalyst layers for polymer electrolyte membrane fuel cells (PEMFC) and electrolyzers (PEMWE) is influenced by various parameters. The impact of these cracks on the device performance remains to be understood. Solvent mixtures used in ink production and the processing of catalyst-coated membranes (CCM), particularly in the drying step, can affect the development of cracks in the catalyst layers. This study presents a novel in-situ investigation of crack formation during an industrially relevant and scalable drying process for catalyst layers. In this regard, locally resolved film temperature and optical crack analysis were conducted simultaneously and in-situ during drying. Cracking is detected when the film consolidates, indicated by a temperature increase and the change in optical layer appearance. Different crack patterns for catalyst inks depending on the initial solvent composition are found and analyzed. Higher 1-propanol content in catalyst inks exhibits faster drying behavior under identical convective drying conditions and more pronounced crack formation, indicated by higher total crack area and larger crack morphologies.

* Corresponding author.
E-mail address: nadine.zimmerer@kit.edu (N. Zimmerer).

https://doi.org/10.1016/j.colsurfa.2025.138807
Received 6 August 2025; Received in revised form 9 October 2025; Accepted 26 October 2025
Available online 30 October 2025

1. Introduction

The formation of cracks is a phenomenon observed across various fields, ranging from the development of cracking in mud and ceramics [1,2], to those found in paintings [3,4], in medical diagnostics [5], and in thin functional layers used in energy applications [6–11].

The formation of cracks during the fabrication process, particularly during the drying step, of catalyst-coated membranes (CCM) for polymer electrolyte membrane fuel cells (PEMFC) and electrolyzers (PEMWE) is a frequently observed phenomenon at both laboratory and industrial scales. The CCM is functional with cracks [12], but performance and especially durability are impaired in the case of larger defect areas [13]. In operation, due to uneven water distribution (including flooding) and heat development, the mass transport of the reactants is inhibited and catalyst utilization is reduced, which affects the overall performance of the system and can lead to accelerated degradation of the membrane. The effects of cracking can lead to the ultimate failure of the membrane and thus to gas leakage [9,13–15]. According to Stoll et al. [13], smaller uncoated, similar to cracked, areas ($\leq$ 4 % of the total electrode surface) have only a minor and therefore tolerable influence on the performance. Initial investigations have also shown that guided cracks can have a positive effect on mass transfer and thus the performance of the system [16,17]. However, most studies agree that cracking of catalyst layers should be avoided.

Nevertheless, the manufacturing conditions that lead to cracking during the drying process are not yet fully understood. In this study, the formation of cracks is investigated experimentally in-situ during catalyst layer drying and coupled with the drying progress to expand the understanding of crack formation in catalyst layers.

1.1. Crack formation in catalyst layers

The formation of cracks in catalyst layers for PEMFC and PEMWE is a known phenomenon that has so far mostly been described empirically. Fractures occur when critical stresses in the system are exceeded. Cracks usually form at the critical point in the drying process when the evaporation front (liquid-vapor interface) moves into the porous network (after the end of film shrinkage) [9,18]. Once the evaporation front has retracted into the system, capillary forces become predominant. Here, the pores empty according to their size due to capillary forces, with larger pores emptying at the expense of smaller ones [18,19]. These inequalities lead to increasing tensile stresses in the pore system, which can range from deformation of the pores to cracking in the macroscopic range [18].

The causes of the critical stress peaks depend on a variety of factors. According to the Griffith criterion, the critical stress depends on the particle size, the particle volume fraction and the shear modulus of the particles, besides the coordination number of the material, the layer thickness and the solvents used [20]. A prediction of crack formation, e. g. using the critical crack thickness (CCT) according to Singh and Tiriumkudulu [20,21] for stress- and stain-limited systems, is possible for model material systems. However, catalyst inks, which are composed of several components including carbon-based catalyst, ionomer, and alcohol/water mixtures, are much more complex multicomponent systems.

In addition, different effects during processing, such as the selectivity of drying, must also be considered. The selectivity of the solvent evaporation describes the relative enrichment or depletion of one solvent in the drying film. Depending on the initial solvent composition and the drying parameters, such as temperature, air flow and water or alcohol concentration in the drying air, the (initial) solvent composition of the film is changing during the drying process [9,22]. Depending on both the thermodynamics and gas kinetics during evaporation, there is a certain (initial) composition of the catalyst ink, where no relative enrichment or depletion of the evaporating components takes place in the liquid phase during drying. This composition is called arheotropic composition for the given drying boundary conditions [22,23]. These evaporation characteristics decisively influence the evolving solvent composition within the layer during drying, thereby influencing particle and ionomer (self) interactions as well as the properties of the ink [9,11,24]. Additionally, the solvent composition affects the wet-bulb temperature of the film during the initial drying phase [25].

In addition to the particle and material properties, which are considered in the Griffith criterion, evaporation rate, catalyst-ionomer interaction, unbound ionomer, defects such as agglomerates, bubbles, pinholes and substrate-ink interactions (e.g. swelling) influence crack formation in catalyst layers for PEMFC [4,11,14,26]. These parameters are coupled with each other in many ways. For example, the drying conditions influence the solvent composition in the catalyst film. The solvent composition in the drying film in turn influences the (self) interaction potential of the ionomer and the catalyst and thus the ionomer coverage of the catalyst [9,27,28]. Scheepers et al [9]. found in their investigation about the drying behaviour of catalyst layers with different (initial) ink compositions that a lower 1-propanol content and thus a higher water content in catalyst layers leads to more pronounced cracking even at smaller layer thicknesses.

When analysing the cracks, a distinction can be made between different types of cracks. Depending on the stresses in the system, I-, U-, V-, T- or Y-shaped cracks form. The I-shaped crack (linear) is the simplest crack form, from which the other crack forms develop in successive crack generations [10,29,30]. The stress and consequent crack morphology within the layers are influenced by the previously described properties of the solids, their interactions, and the process parameters. With constant ink formulation and processing conditions, the layer thickness emerges as a critical factor for the crack morphology [8,10].

Cracking in catalyst layers could be successfully reduced by adding a high boiling point solvent such as ethylene glycol or propylene glycol [11,31]. Another approach is the addition of additives such as carbon nanotubes or polymeric additives to reduce cracking [8,29]. Nevertheless, depending on the ink components, the addition of additives may not be suitable or may lead to undesirable effects during processing or fuel cell operation.

2. Materials and experimental section

2.1. Ink preparation

Inks were prepared using Tanaka TEC10EA50E catalyst (Tanaka Kikinzoku Kogyo K.K, Ja-pan) with a platinum loading of 47 wt%, Nafion dispersion D2020 (Chemours, USA), and an alcohol/water solvent mixture. The inks comprised of 1-propanol (Carl Roth GmbH & Co. KG, Germany) and ultrapure water as solvents. In this study, two solvent compositions in the inks are compared (see Table 1): firstly an ink containing 53 wt% 1-propanol and 36 wt% water (P-Ink) and secondly an ink with 18 wt% 1-propanol and 71 wt% water (W-Ink). The pure solvent compositions of the P-Ink are 60:40 (in wt%) and W-Ink with 20:80 (in wt%) 1-propanol to wa-ter, respectively. Under the applied drying conditions, the arheotropic composition of the sol-vent mixture (excluding solid ink components) is $x_{P,AR} = 63$ wt% (and $> x_{P,0}$ of both P- and W-Ink).

Table 1
Ink formulation of the two dried catalyst inks: P-Ink consists of a higher 1-propanol content of $x_{P,0} = 53$ wt% and the W-Ink has a lower 1-propanol content of $x_{P,0} = 18$ wt%, but higher water content ($x_{W,0} = 71$ wt%).

Ink component	Mass ratio / wt%	P-Ink		W-Ink	
		Ink	Solvents	Ink	Solvents
Catalyst	$x_{C,0}$	7		7	
Ionomer	$x_{I,0}$	4		4	
1-Propanol	$x_{P,0}$	53	60	18	20
Water	$x_{W,0}$	36	40	71	80

In both inks, the 1-propanol concentration was below the arheotropic concentration for the applied drying parameters, meaning a relative depletion of 1-propanol in the film is expected during the drying process [22,23]. The ionomer to carbon ratio (I/C) was 1.0. All components were processed into a catalyst ink for 3 h at 1000 rpm using a dissolver CN10 equipped with a ball mill unit APS 250 (VMA Getzmann GmbH, Germany).

2.2. Coating and drying of the catalyst layer

The inks were coated onto a 50 μm thick PTFE substrate (Hightechflon, Germany) at a coating speed of 10 cm/s using a doctor blade (ZUA2000, Zentner, Switzerland). The ink was then dried using a Comb Nozzle Dryer with a honeycomb nozzle field (CN Drying Technology GmbH, Germany). The convective drying air temperature was set to $T_{conv} = 72$ °C and the heat transfer coefficient was $\alpha = 35$ W m^{-2} K^{-1}. The water pre-loading of the drying air was $\widetilde{y}_{W,\infty} = 0.009$ (also being: relative humidity $RH = 28.5$ % at 25 °C or dew point $\tau = 5.5$ °C). By periodically moving the drying nozzles, the drying was homogenized.

A PI 400i infrared (IR) camera (Optris, Germany) and a digital single lens reflex (DSLR) camera (Nikon D5600 with lens Sigma Zoom 17–55 mm, Japan) were integrated into the drying setup. This enables the in-situ monitoring of crack formation during drying by analyzing greyscale image data. A defined 0.2 × 0.2 mm^2 region within the catalyst layer was evaluated at specific drying times using the image processing program ImageJ. Greyscale intensity, ranging from 0 (black) to 255 (white), was assessed by extracting minimum, maximum, and mean values. Cracks were observed through the PTFE foil. With the used illumination settings, cracks that reach to the substrate can be detected (surface cracks are not visible). An increase in mean and maximum intensity indicates crack formation, as cracks appear brighter under the applied illumination conditions. Additionally, the IR camera was used to analyze local temperature profiles across the film area during drying. This innovative setup allows both, real-time observation of crack formation and its correlation to the drying process in form of spatially resolved film temperature distribution analysis. More detailed information on the experimental setup can be found in Fig. 1.

The dried catalyst layers where characterized by measuring layer thickness using the gauge ID-H0530 (Mitutoyo, Japan) and by microscopic image stitching using a VHX-7000 microscope (Keyence, Japan) with 100 × magnification and backlight illumination.

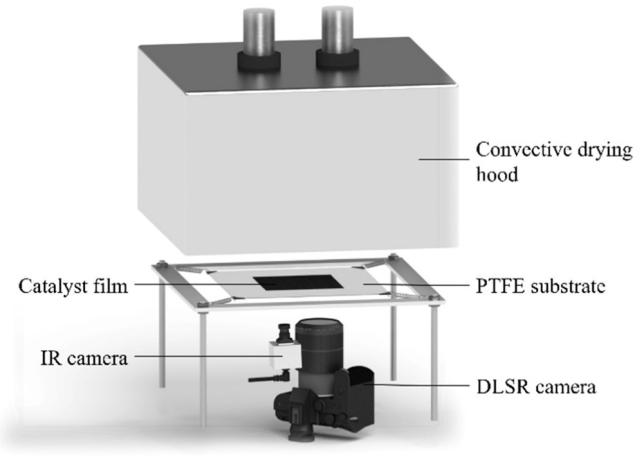

Fig. 1. Schematic illustration of the experimental setup for convective drying of the catalyst film with integrated in-situ infrared temperature (IR camera) and crack detection (DSLR camera).

3. In-situ investigation of crack formation and drying of catalyst films with different ink formulations

3.1. Interrelation of crack formation and drying of catalyst films

The integration of two cameras into the experimental setup for defined catalyst layer drying allows for simultaneous and in-situ observation of both, the drying process and crack formation with sufficient spatial resolution over the entire catalyst layer area. This is particularly important as cracks are local phenomena, often resulting from local inhomogeneities in the energy input during drying, the substrate or the ink. Correlating the drying progress with crack formation offers valuable insights into potential underlying mechanisms of crack initiation.

The drying and cracking behavior of the two ink formulations, which differ in their initial solvent composition, are examined in this study. The objective is to systematically analyze the process- and ink formulation-related factors influencing crack formation through a comparative analysis of the camera images at respective time intervals during the drying process.

Fig. 2 shows the DSLR camera images of a forming catalyst layer of the P-Ink (higher initial 1-propanol mass fraction of $x_{P,0} = 53$ wt%) during the convective drying at an air temperature of $T_{conv} = 72$ °C with a dew point of $\tau = 5.5$ °C (first row). The second row shows the temperature distribution across the same area of the catalyst layer which was simultaneously detected by the IR camera. Both, camera and IR camera recordings are shown in 10-second intervals beginning at the first color change—indicating a deviation from the initial wet-bulb temperature within the film during the constant rate period of drying process—observed in the infrared (IR) camera images. In the first row, cracks are visible as bright spots in the applied illumination conditions. The catalyst layer appears initially dark grey. The film temperature (second row) over the entire surface of the catalyst layer is represented by a color scale. The temperature scale in the IR camera pictures ranges from 15 °C (blue) to 80 °C (white) and is determined using infrared thermography.

Although the drying process was homogenized to a large extent by periodically moving the drying nozzles across the catalyst layer, local inhomogeneities persist throughout the film drying. Fig. 2 presents an overview of the entire electrode during drying. As crack formation is a highly localized phenomenon, specific regions of the layer are examined in greater detail in subsequent analyses.

At the beginning of the drying process, the DSLR camera shows a uniformly black catalyst film across the entire electrode area (0 s). Concurrent thermal analysis reveals also a spatially uniform temperature distribution across the surface, recording a wet bulb temperature of 25 °C (purple). The first local color change in both the DSLR and IR camera images occurs after 26 s, appearing as a circular spot at the left center of the catalyst layer. In the DSLR picture the color changes from dark grey to a lighter grey, which is due to the transition from wet catalyst ink to the dry catalyst layer. The IR image shows a temperature increase of the same area from the wet bulb temperature at approx. 26 (purple) to 40 °C (red), indicated by the colour change from purple to red. During the initial phase of the drying process (purple), the catalyst layer remains at the wet-bulb temperature, resulting from the equilibrium between convective heat input and evaporative cooling. As drying progresses, more dry areas occur across the electrode (colour changes from black to grey in the DSLR and from purple to orange in the IR images) until the entire electrode is fully dried. Interestingly, although cracking is a localized phenomenon, the resulting cracks are uniformly distributed throughout the dried catalyst layer. No indication of the cracking onset is observable in the final electrode.

The progression of crack formation over time is investigated by correlating the greyscale distribution of the catalyst layer with the corresponding local film temperature (purple) at an exemplary position in the catalyst layer during drying (Fig. 3). Since cracking is a local

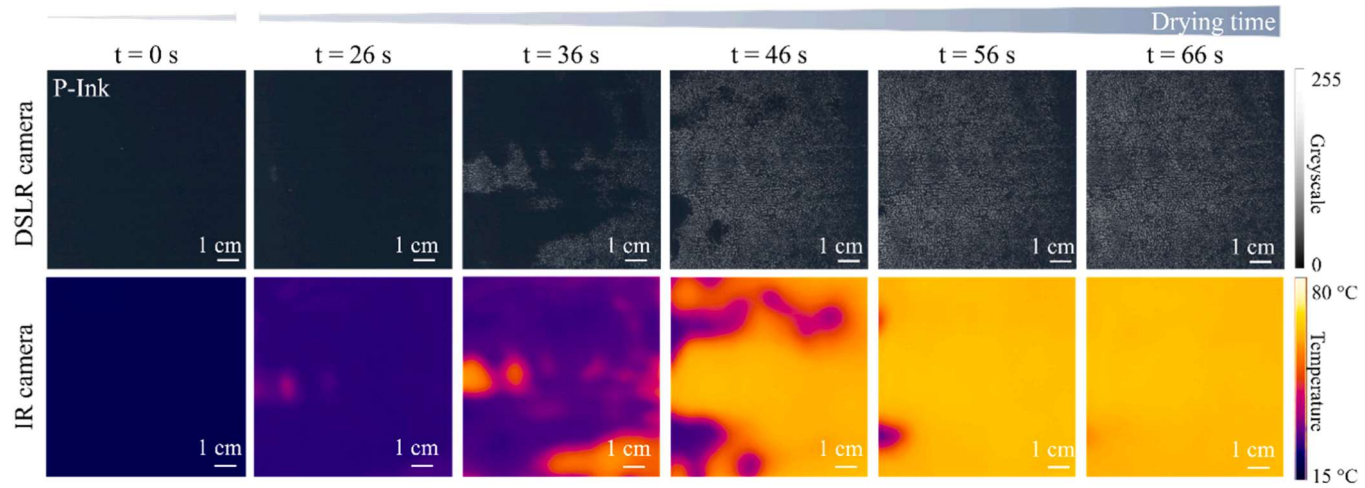

Fig. 2. In-situ DSLR camera recordings (first row) and IR temperature distributions (second row) at different drying times during drying (0 – 66 s) of a catalyst layer produced from the P-Ink (with initial 1-propanol content of $x_{P,0} = 53$ wt%). Convective drying was applied with an air temperature of $T_{conv} = 72$ °C, $\alpha = 35$ W m^{-2} K^{-1} and an air dew point of 5.5 °C. Cracks appear as bright spots in the DSLR camera pictures. The temperature recorded ranges from 15 °C (blue) to 80 °C (white). Cracks and local film temperature changes are detected.

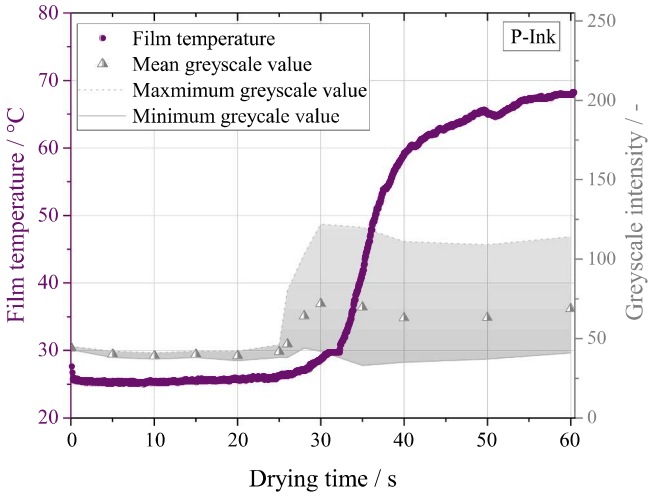

Fig. 3. Local temperature measurement (by IR thermography, purple) and greyscale analysis (DSLR camera, grey) of an exemplary section (200 × 200 μm^2) of Fig. 2 during the convective drying of the catalyst layer produced from P-Ink ($x_{P,0} = 53$ wt%). Greyscale intensity analysis involves evaluating the minimum, maximum, and mean values within the greyscale distribution, ranging from 0 (black) to 255 (white). A (sharp) increase in the mean and maximum value indicates a higher number of brighter pixels (cracks). It is observed that cracking coincides with the start of the temperature rise.

phenomenon, an analysis over a larger area than in this investigation (200 ×200 μm^2) is not practical. Crack formation is identified using the analysis of the greyscale intensity distribution (ranging from 0 (black) to 255 (white)) within the selected region. From this distribution, the minimum, maximum, and mean greyscale values are extracted. An increase in the proportion of bright pixels, which is caused by the presence of cracks, results in a corresponding rise in the mean and maximum greyscale values. The mean greyscale intensity is represented by data points in the diagram, while the shaded area between the maximum and minimum detected grey values illustrates the distribution range of grey shades across the sample. The histograms representing the greyscale intensity distribution for an exemplary film during the drying process (W-Ink, Fig. 5) are provided for three representatives times in the supporting information S1.

The film shows an initial temperature plateau at 25.4 °C. A rise in temperature is observed starting 26 s after the start of drying. As drying concludes, the catalyst layer temperature reaches 68.8 °C. The mean greyscale values remain constant up to 26 s with small deviation observable. After 26 s, the mean and maximum values begin to increase, indicating crack formation, as a higher number of brighter pixels is detected. At 30 s, a plateau is reached, suggesting that crack formation is completed. Notably, the increase in bright pixel intensity coincides with the increase in film temperature, indicating a correlation between the drying progress and the start of crack formation. Cracks are detected as the film temperature begins to rise from the wet-bulb temperature. This observation suggests that cracks in catalyst layers typically form shortly after the evaportion front retreats into the pore network and capillary forces arise . This aligns with established models in the literature [19, 20]. As evaporation in the porous electrode progresses, film-side resistances have an impeding influence on evaporation and the film temperature increases.

In this ink and with the applied drying conditions, cracking appears to be complete within only 4 s. This extremely short timescale would necessitate precise control of process parameters to avoid cracking solely from the process side, e.g., by decreasing the drying rate at this critical stage.

Next, the cracking behavior during the drying process is analyzed for another ink formulation. The main distinction between this new ink formulation and the previously studied P-Ink lies in the composition of the solvent mixture (see Table 1). Specifically, the P-Ink formulation contains 53 wt% 1-propanol, whereas the W-Ink formulation contains only 18 wt% 1-propanol. These differences in solvent composition are expected to influence the drying kinetics and the resulting solvent composition in the layer. Furthermore, the differences in (initial) solvent composition may change the (self-)interactions between the ionomer and particles.

In Fig. 4, the DSLR camera images (first row) and temperature distribution (second row) for a film cast from the W-Ink is shown at relevant time intervals. To ensure comparability with the previous study, identical drying parameters were applied: drying air temperature $T_{conv} = 72$ °C, $\alpha = 35$ W m^{-2} K^{-1}, and air dew point $\tau = 5.5$ °C. At the beginning of the drying process, a uniform catalyst film is observed in both the DSLR camera image (black) and the IR image (purple). The catalyst film remains in the constant rate period at the wet-bulb temperature. The coloration in the IR image (more blueish purple than in Fig. 2) arises from the higher wet-bulb temperature, which is influenced by the initial composition of the solvents present in the layer. A detailed examination of the temperature profiles and drying kinetics is given in

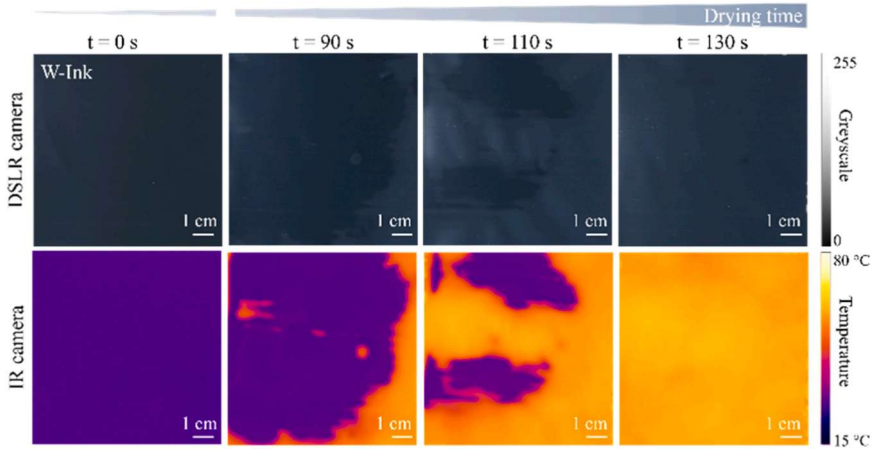

Fig. 4. In-situ DSLR camera recordings (first row) and IR temperature distributions (second row) at different drying times during drying (0–130 s) of a catalyst layer produced from the W-Ink (with initial 1-propanol content of xP,0 = 18 wt%). Convective drying was applied with T_{conv} = 72 °C, α = 35 W m-2 K-1 and an air dew point of 5.5 °C. Cracks appear as white spots in the DSLR camera pictures. The temperature range recorded ranges from 15 °C (blue) to 80 °C (white). Cracks and local film temperature changes are detected.

chapter 3.2.

As drying progresses, the optical appearance of the catalyst film captured by the DSLR camera transitions from black to grey. Simultaneously the corresponding infrared recording changes from purple to orange, indicating a temperature increase from the wet-bulb temperature. Cracking appears to be less pronounced in the aqueous-based ink formulation (W-Ink) compared to the previously studied P-Ink, which contained a higher concentration of 1-propanol. Due to the fewer occurrence and reduced size of cracks in the W-Ink layers, their detection in DSLR images (as shown in Fig. 4, upper row) is significantly more challenging. For enhanced in-situ crack analysis of these small crack structures, a microscope could be integrated into the setup. However, this would limit the analysis to a small, unrepresentative and potentially uncracked area of the catalyst layer. Therefore, to enable reliable detection of crack formation, again greyscale intensity analysis was performed on a representative area of the electrode surface and

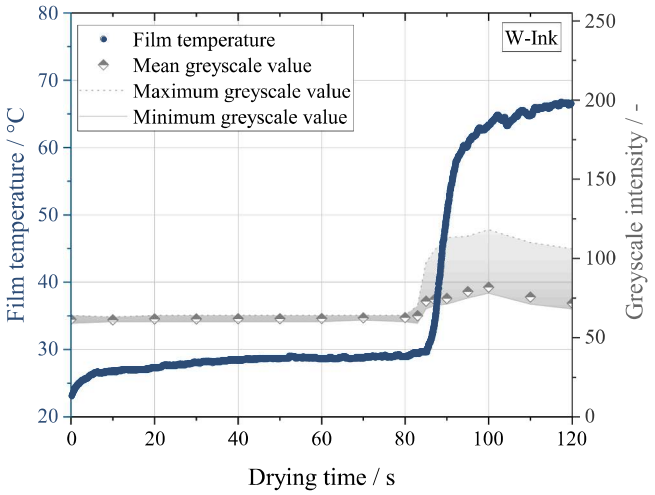

Fig. 5. Local temperature profile conducted via IR thermography (blue) and greyscale analysis (grey) of the DSLR recording of an exemplary section (200 ×200 μm^2) during the convective drying of the catalyst layer produced from W-Ink ($x_{P,0}$ = 18 wt%). Greyscale intensity analysis involves evaluating the minimum, maximum, and mean values within the greyscale distribution, ranging from 0 (black) to 255 (white). A (sharp) increase in the mean and maximum value indicates a higher number of brighter pixels (cracks). It is observed that cracking coincides temporally with the start of the temperature rise.

correlated with the (local) drying progress, as indicated by the change in film temperature (Fig. 5).

Both, the film temperature and the greyscale intensity show an initial plateau during the constant rate period of the catalyst film drying. Initially, the catalyst layer dries at a wet-bulb temperature of 26.9 °C. At 84 s, the film temperature shows an increase followed by a rapid rise to 66.6 °C. Again, at the onset of the temperature increase, a change in the greyscale intensity is observable. All characteristic values derived from the greyscale intensity analysis (minimum, mean, and maximum) exhibit a noticeable elevation starting at 83 s. After only 2 s (at 85 s), the grey value stabilizes at a higher plateau level.

Notably, the optical change in the catalyst film associated with progressing drying is also captured by the greyscale intensity analysis. While the mean greyscale intensity shows a marginal increase of less than 2 % during the initial plateau phase, this change cannot account for the sharp increase in grey value intensity (17 % for the W-Ink and 65 % for the P-Ink) occurring subsequentially. Therefore, this is defined as the start of crack formation within the catalyst layer.

The coupled analysis of drying and crack formation was also performed at multiple locations within the individual catalyst layers and in further experiments under identical drying conditions for both ink formulations. To further validate the previously identified onset of crack formation during the drying process, additional experiments were conducted with varied air temperatures. A selection of these results is provided in the supporting information S2. With all investigated inks and drying conditions, a consistent temporal correlation was observed between the (local) increase in film temperature from the wet-bulb temperature and the rise in the greyscale intensity values change. Additionally, in a different experimental setup confocal line laser distance measurements revealed the end of film shrinkage coinciding with crack initiation. Crack formation was observed as pronounced fluctuations in layer thickness and confirmed by simultaneous microscopic imaging. These results, which will be presented in a separate publication, reinforce the findings that the critical time for crack formation during drying is at the transition to the evaporation from the porous network of the catalyst film.

Previous studies modeled the selective drying behavior of catalyst films, providing a comprehensive framework for understanding film drying and forming the basis for tailoring drying protocols to specific ink formulations with the aim of minimizing crack formation [22,32]. Exemplary processing strategies to enhance film properties have already been successfully implemented in battery electrode manufacturing through multi-stage drying processes [32–34].

In an additional study, film height measurements in-situ during

drying also found the end of film shrinkage coinciding with the crack initiation. Cracking was identified as pronounced fluctuations in layer thickness and confirmed by simultaneous microscopic imaging. However, these results will be focus of a separate publication but strengthen the finding of this study, identifying the critical time for crack formation at the start of film temperature increase from the initial tempertaure plateau which also coicides with the end of film shrinkage. Previous studies modeled the selective drying behavior in catalyst films providing a comprehensive understanding of film drying and provide the basis for tailoring drying protocols to specific ink formulations with the goal of minimizing crack formation. Similar strategies for improved film properties have already been successfully employed in battery electrode manufacturing through the implementation of multi-stage drying processes [33–35].

3.2. Drying behavior of the catalyst films

As observed by the previous analysis, variations in the drying behavior of films with differing initial solvent compositions are detectable. The catalyst layers during drying differ in film temperatures within the coated electrode area, and thus also the local drying time. It is notable that the drying of the P-Ink is almost twice as fast when dried with identical drying parameters. This behavior can be attributed to differences in the drying kinetics of the specific catalyst inks and the differences in the thermodynamics of the evaporation of 1-propanol/water mixtures at different solvent compositions.

A comparison of the film temperature as a function of drying time of the two investigated coatings with 53 wt% und 18 wt% initial 1-propanol content is plotted in Fig. 6. For this analysis, the entire catalyst-coated area was evaluated, and the minimum temperature within this region is displayed over the drying period. The minimum temperature serves as an indicator for the completion of the drying process across the entire film, even in the presence of slight spatial inhomogeneities, and can therefore be considered a representative measure of the overall drying time in the experimental setup used.

The P-Ink, with an initial composition of $x_{P,0} = 53$ wt%, shows a plateau in minimum film temperature at 25.1 °C . In contrast, the W-Ink exhibits a higher minimum film temperature of 27.2 °C during this drying stage. Subsequently, the film temperature of both inks rises, ultimately approaching the convective drying air temperature, with average final film temperature of 62 – 65 °C. The drying process is noticeably dependent on the solvent composition. While the film casted from the P-Ink shows a fully dried catalyst layer after 71 s, the W-Ink layer requires significantly more time, exhibiting a 91 % longer drying time of 132 s. The observed differences in the drying rate of the tested layers from the two different inks can be attributed to the evaporation behaviour of the 1-propanol/water solvent mixture of the catalyst ink.

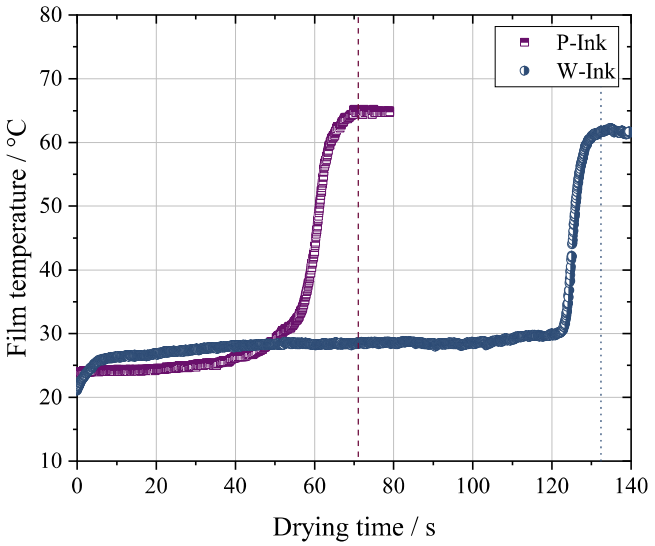

Fig. 6. Time-resolved monitoring via IR thermography of the minimum film temperature during convective drying ($T_{conv} = 72$ °C, $\alpha = 35$ W m^{-2} K^{-1} and $\tau = 5.5$ °C) conducted for films from inks with initial 1-propanol solvent content of 53 wt% (P-Ink, purple) and 18 wt% (W-Ink, blue). The temperature plateaus correspond to the wet-bulb temperatures of the catalyst inks in constant rate period. The veritical lines indicates the end of the drying process of the catalyst films.

The composition of the alcohol/water mixture in the inks significantly influences the thermodynamics of the evaporation process, thereby affecting both the wet-bulb temperature and the drying rate. In addition to the thermodynamics, gas-phase transport kinetics must also be accounted for, as they also contribute to changes in solvent composition during drying (selective evaporation). An analytical investigation of the drying process is conducted below to show the effects of selective evaporation.

For the applied drying parameters in the experiments, the wet-bulb temperatures and corresponding drying rates for different mixture compositions (shown as 1-propanol mass fractions of the solvent mixture) are presented in Fig. 7. Additionally, the anticipated changes in solvent composition during catalyst film drying, resulting from selective evaporation, are indicated in blue for the W-Ink and in purple for the P-Ink. The arrows denote the direction of composition change; however, their lengths do not represent the drying time.

In this analysis, mass transfer kinetics is described using Fick's law and the thermodynamics is calculated with Raoult–Dalton's law. Wagner's equation is used for the vapor pressure and the activity coefficients of the binary mixture is included with the van Laar model. The solid component of the inks were excluded from this analysis, as their influence on solvent evaporation during the constant rate period is negligible.

The calculated wet-bulb temperatures of the pure solvents are 26.9 °C for water and 30.4 °C for 1-propanol under the specified, adiabatic drying conditions ($T_{conv} = 72$ °C, $\alpha = 35$ W m^{-2} K^{-1} and $\tau = 5.5$ °C). For the mixture of both solvents, the wet-bulb temperature is lower than that of the pure components, showing a plateau at 23.8 °C across a broad range of compositions. Pure water exhibits the lowest calculated drying rate (0.6 g m^{-2} s^{-1}), while pure 1-propanol shows the highest (1.8 g m^{-2} s^{-1}). The drying rates of the mixtures lie between these extremes, varying with composition. A nearly constant plateau is noticeable at 1.1 g m^{-2} s^{-1}. The shape of the curve showing the drying rate depending on the solvent composition is derived from the thermodynamics of the evaporation behavior of the 1-propanol/water mixture in particular.

When selective evaporation of the catalyst layer is considered, pronounced differences in drying rate and film temperature are observed. For the W-Ink with an initial 1-propanol composition (excluding solids) of 20 wt% (see Table 1), the 1-propanol is preferentially evaporated which leads to a depletion of alcohol in the drying film. According to drying simulations of the film, after about half of the drying time almost exclusively water is expected to remain in the film [32]. The evaporation of mainly water significantly reduces the drying rate, primarily due to the resulting thermodynamic changes [22,23,36,37]. The slower drying rate leads to initially higher film temperatures during drying.

In contrast, the P-Ink, with an initial solvent composition of 60 wt% 1-propanol (excluding solids), undergoes smaller changes in solvent composition during drying compared to the W-Ink. The initial mixture composition is located within the plateau region for both drying rate and wet-bulb temperature. As a result, variations in drying rate and wet bulb temperature aren't as significant throughout the drying. The impact of solvent composition on the selectivity of the drying process in these systems has been investigated in a previous study by our group [22].

This distinct evaporation behavior of catalyst ink solvents explain the observed differences in drying time and film temperature between the W- and P-Ink layers. The measured and calculated film temperature in

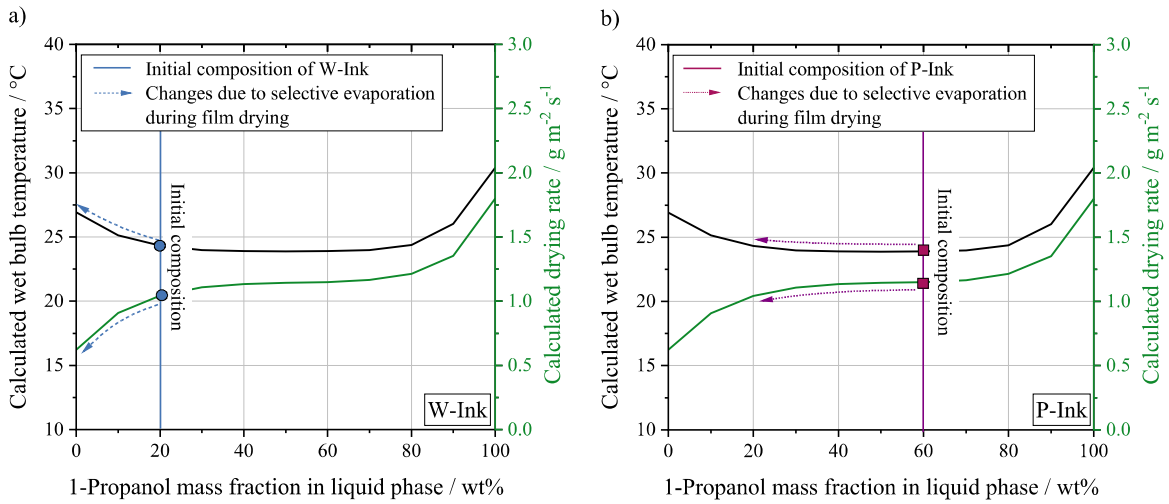

Fig. 7. Calculated wet bulb temperature (black) and drying rate (green) at different solvent compositions of a binary 1-propanol/water mixture dried with convective drying parameters of $T_{conv} = 72$ °C, $\alpha = 35$ W m^{-2} K^{-1} and $\tau = 5.5$ °C. a) shows the changes in solvent composition due to selective evaporation of the W-Ink, b) the composition changes of the P-Ink during catalyst film drying. The length of the arrows are not indicating the drying time, but the compositional changes during drying.

the constant rate period, taking selective solvent evaporation into account, differ by only 2 ± 1 %.

Additionally, the (self-)interactions between the ionomer and the catalyst are affected by the composition of the dispersing solvents. Thus, variations in concentration (also during the drying process itself) may have an impact on the electrode structure and crack formation [9,14,27,38].

4. Ex-situ investigation of crack patterns in catalyst layers

As outlined in the preceding chapters, the drying behavior of the inks varies significantly based on their initial solvent composition. Another critical characteristic analyzed in this study is the formation and morphology of cracks depending on the ink composition.

The crack patterns of the catalyst layers are analyzed to infer about the crack size, branching and total crack area. Representative microscopic pictures of the previously described layers are shown in Fig. 8. The images a) and b) show stitched microscope images taken in backlight illumination. Cracks appear white, the catalyst layer black. High-resolution images of the cracks with incident lighting are also shown (c, d).

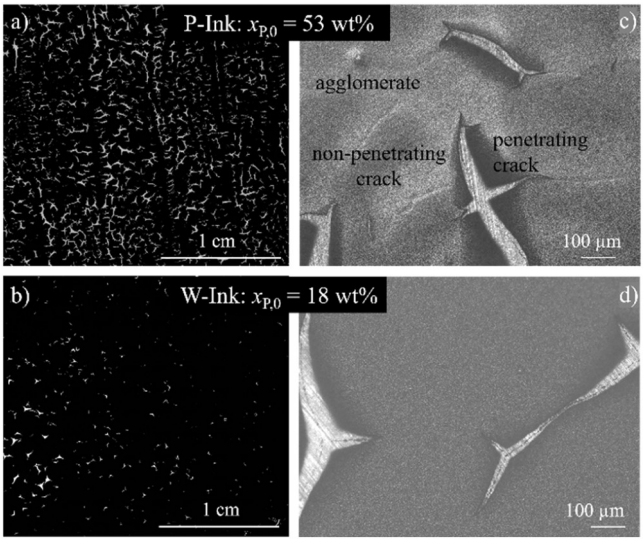

Fig. 8. Stitched microscope images of the dried electrodes processed with the P-Ink (a) and W-Ink (b) taken with backlight illumination, and detailed microscopic images with top-light illumination of representative crack formations for both catalyst layers of the P-Ink and W-Ink (c, d). The drying conditions and layer thicknesses were adjusted identical for this ex-situ investigation.

The P-Ink layers tend to form lager and more pronounced cracking during the drying process, resulting in a network of branched, yet unconnected cracks across the entire coated area. The average crack area in the selected images is 1.1 % for the P-Ink in Fig. 8a). The layer thickness of the P-Ink electrode is 9.5 ± 1.4 µm. The W-Ink exhibits fewer, smaller, and less branched cracks with 0.4 % crack area for a layer thickness of 9.6 ± 1.0 µm (Fig. 8b). Thus, the total crack area in P-Ink electrodes is 175 % larger than in W-Ink electrodes. For this analysis, it is essential to compare layers of identical thicknesses, as layer thickness represents one of the most critical factors influencing crack formation [8,10,20].

The P-Ink layers show cracks with multiple branches originating from a primary crack. In most analyzed spots, the crack structures exhibit four or more branching points. Smaller cracks generally exhibit fewer branches and are similar to T- or Y-shaped cracks, as classified by Kumano et al [10]. The width of the cracks is up to 40 µm. The majority of cracks have a length of ≤ 1.6 mm, but some larger cracks are observed on the left side of the electrode, where minor variations in layer thickness are present. No primary orientation of the cracks can be recognized, indicating isotropic stress within the catalyst layer.

The W-Ink layers show only isolated cracks, which are categorized as V-shaped or Y-shaped. Most of the cracks are significantly smaller and thinner and less branched compared to those observed in the P-Ink layers. The length of most of the cracks is with ≤ 0.5 mm considerably shorter than in the P-Ink layers at similar thicknesses.

The surface morphology of the catalyst layers also exhibits notable differences, as evident in the detail images (c, d). The W-Ink layer displays a homogeneous surface, whereas the P-Ink layer shows agglomerates and non-penetrating cracks, which don't diverge and are most probably not extending to the substrate. Top-view and cross-sectional scanning electron microscopy (SEM) were performed for a more detailed analysis of cracking in the P-Ink layer (Fig. 9).

The top-view image (Fig. 9a) shows a crack originating at an agglomerate and propagating in three directions, separated by angles of approximately 120°. Local delamination of the layer in the vicinity of the agglomerate is also evident. Crack formation frequently starts at agglomerates, where drying-induced stresses accumulate. Other

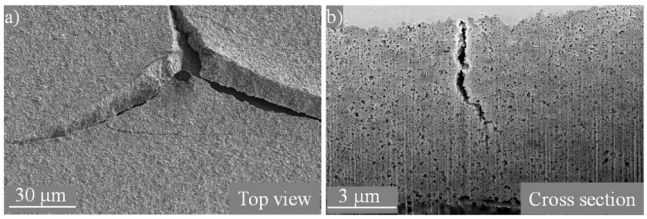

Fig. 9. Scanning electron microscopy (SEM) images of cracks in catalyst layers: (a) top-view image showing a crack originating from an agglomerate; (b) cross-sectional view revealing a crack initiating at the top of the catalyst layer without propagating to the substrate.

heterogeneities that can induce cracking include entrapped air bubbles and impurities in the ink or at the substrate surface. Such irregularities should be minimized during ink formulation and film processing to mitigate crack formation. The cross section SEM image (Fig. 9b) of the catalyst layer represents a crack that does not penetrate to the substrate. Cracks typically initiate at the top surface of the catalyst film. They are caused by solvent evaporation which induces film shrinkage. The adhesion of the film to the substrate constrains three-dimensional film shrinkage, resulting in biaxial tensile stresses in plane of the catalyst film. When these accumulated stresses exceed the mechanical film stability, which was determined during this study at the end of film shrinkage, cracks initiate at the film surface. In-plane crack growth generally occurs perpendicular to the principal stress field in regions of comparatively lower local stress concentration [19,21,39].

Cracks which do not penetrate to the substrate are observed in ex-situ microscopy but remain undetectable during in-situ analysis during film drying. As crack initiation and propagation are completed within only a few seconds, through-plane crack growth is not expected to significantly affect the results presented. During PEM system operation, these weaknesses may further expand due to swelling and shrinkage, potentially leading to performance losses and material degradation.

Crack formation is strongly influenced by (initial) solvent composition. In this study and under the drying conditions applied, catalyst layers produced from the P-Ink exhibit more pronounced cracking compared to those with lower initial alcohol content (W-Ink). In literature, different catalyst systems show differing tendencies with respect to cracking behavior with a higher 1-propanol content in the ink. Some studies, such as those by Kumano et al. [10], Park et al. [40], and this study, report an increase in cracking with elevated 1-propanol contents, while others, like Scheepers et al. [9], observe a reduction in cracks in the catalyst layers. However, the variability in catalyst systems, ionomers, and drying conditions resents significant challenges for the comparison of the results in this context.

Cracks in the catalyst layers critically affect both the performance and lifetime of PEM fuel cells. Their impact depends on crack size, density, and location, making a precise control of crack formation in catalyst layers essential. While small cracks can initially enhance mass transport, they generally accelerate water accumulation, increase mass transfer resistance, and cause uneven current distribution, resulting in significant performance losses over time. Cracks also promote mechanical and chemical degradation, ultimately reducing the lifetime of the PEM system [13,16,17].

This study contributes to a comprehensive understanding of crack formation during catalyst layer processing, aiming to guide the development of optimized processing strategies to control crack morphology. Strategies for crack mitigation should, for example, focus on ink formulation, processing of ink and catalyst layers. Especially exploiting the selective evaporation behavior of catalyst films, preloading the drying air with solvents to control the drying selectivity could be a powerful tool for crack mitigation.

5. Conclusion

By integrating a digital single lens reflex (DSLR) and an infrared (IR) camera into an experimental drying setup, in-situ investigations of crack formation during the drying process of catalyst layers for PEM fuel cells and electrolyzers were conducted. Two ink formulations with identical catalyst material, ionomer-to-catalyst ratio (I/C), and ink processing were produced. The only difference in the inks was the composition of the dispersing solvents. The P-Ink had an initial composition of 53 wt% 1-propanol, 36 wt% water, and 11 wt% solids, whereas the W-Ink consisted of 18 wt% 1-propanol, 71 wt% water, and 11 wt% solids.

In-situ analysis of crack formation demonstrated that cracks could be reliably detected in both ink formulations via greyscale intensity analysis, and correlated with the film's thermal profile during drying. The start of crack formation consistently coincided with the rise in film temperature during drying. This temporal correlation was reproducible for both inks also under varying drying conditions.

Additionally, the layers produced from the P-Ink dried significantly faster than the ones from the W-Ink, leading to lower film temperatures under identical drying conditions. These differences are attributed to the distinct evaporation dynamics, mainly the thermodynamics, of the respective solvent mixtures and should be addressed in the design of the drying process on an industrial scale.

The ex-situ analysis of the crack pattern of the dried electrodes also shows differences in crack area and dimensions for the investigated inks. Catalyst layers produced with P-Inks exhibit larger, more branched, yet non-connected crack networks, while W-Inks reveal fewer, smaller, and also isolated cracks. Quantitatively, the total crack area in the P-Ink electrodes is 175 % higher than in the W-Ink electrodes with only being 1.1 % of the total electrode area. The influence of different crack patterns and different processing routes with identical crack pattern on the electrode performance will be focus of subsequent investigations. The ultimate goal of these and following investigations is to precisely adjust crack area, occurrence, and morphology through processing parameters.

CRediT authorship contribution statement

Philipp Quarz: Writing – review & editing, Methodology, Conceptualization. **Linus Janning:** Writing – review & editing, Conceptualization. **Philip Scharfer:** Supervision. **Wilhelm Schabel:** Supervision. **Nadine Zimmerer:** Writing – review & editing, Writing – original draft, Visualization, Validation, Methodology, Investigation, Data curation, Conceptualization.

Declaration of Generative AI and AI-assisted technologies in the writing process

During the preparation of this work, the authors used DeepL (DeepL SE) and ChatGPT (Open AI) to improve readability and clarity. After using these tools, the authors reviewed and edited the content as needed and take full responsibility for the content of the publication.

Declaration of Competing Interest

The authors declare that they have no known competing financial interests or personal relationships that could have appeared to influence the work reported in this paper.

Acknowledgements

The authors would like to thank Dr. Erich Müller form the Laboratory for Electron Microscopy (LEM, KIT) for conducting the scanning electron microscopy.

Appendix A. Supporting information

Supplementary data associated with this article can be found in the online version at doi:10.1016/j.colsurfa.2025.138807.

Data Availability

Data will be made available on request.

References

[1] R.C. Chiu, T.J. Garino, M.J. Cima, Drying of granular ceramic films: I, effect of processing variables on cracking behavior, J. Am. Ceram. Soc. 76 (1993) 2257–2264, https://doi.org/10.1111/j.1151-2916.1993.tb07762.x.

[2] L. Goehring, R. Conroy, A. Akhter, W.J. Clegg, A.F. Routh, Evolution of mud-crack patterns during repeated drying cycles, Soft Matter 6 (2010) 3562, https://doi.org/10.1039/b922206e.

[3] F. Boulogne, L. Pauchard, F. Giorgiutti-Dauphiné, Effect of a non-volatile cosolvent on crack patterns induced by desiccation of a colloidal gel, Soft Matter 8 (2012) 8505, https://doi.org/10.1039/c2sm25663k.

[4] F. Giorgiutti-Dauphiné, L. Pauchard, Painting cracks: a way to investigate the pictorial matter, J. Appl. Phys. 120 (2016) 065107, https://doi.org/10.1063/1.4960438.

[5] MichaelJ. Hertaeg, R.F. Tabor, A.F. Routh, G. Garnier, Pattern formation in drying blood drops, Philos. Trans. R. Soc. A 379 (2021) 20200391, https://doi.org/10.1098/rsta.2020.0391.

[6] J. Kumberg, M. Müller, R. Diehm, S. Spiegel, C. Wachsmann, W. Bauer, et al., Drying of lithium-ion battery anodes for use in high-energy cells: influence of electrode thickness on drying time, adhesion, and crack formation, Energy Technol. 7 (2019) 1900722, https://doi.org/10.1002/ente.201900722.

[7] K. Rollag, D. Juarez-Robles, Z. Du, D.L. Wood, P.P. Mukherjee, Drying temperature and capillarity-driven crack formation in aqueous processing of Li-ion battery electrodes, ACS Appl. Energy Mater. 2 (2019) 4464–4476, https://doi.org/10.1021/acsaem.9b00704.

[8] P. Quarz, N. Zimmerer, A.-M. Steck, P. Scharfer, W. Schabel, Carbon nanotubes (CNT) as an additive towards crack-free catalyst coated membranes (CCM), Int. J. Hydrog. Energy 57 (2024) 789–797, https://doi.org/10.1016/j.ijhydene.2024.01.049.

[9] F. Scheepers, A. Stähler, M. Stähler, M. Carmo, W. Lehnert, D. Stolten, Layer formation from polymer carbon-black dispersions, Coatings 8 (2018) 450, https://doi.org/10.3390/coatings8120450.

[10] N. Kumano, K. Kudo, A. Suda, Y. Akimoto, M. Ishii, H. Nakamura, Controlling cracking formation in fuel cell catalyst layers, J. Power Sources 419 (2019) 219–228, https://doi.org/10.1016/j.jpowsour.2019.02.058.

[11] N. Hasegawa, A. Kamiya, T. Matsunaga, N. Kitano, M. Harada, Analysis of crack formation during fuel cell catalyst ink drying process. Reduction of catalyst layer cracking by addition of high boiling point solvent, Colloids Surf. A Physicochem. Eng. Asp. 628 (2021) 127153, https://doi.org/10.1016/j.colsurfa.2021.127153.

[12] S. Kundu, M.W. Fowler, L.C. Simon, S. Grot, Morphological features (defects) in fuel cell membrane electrode assemblies, J. Power Sources 157 (2006) 650–656, https://doi.org/10.1016/j.jpowsour.2005.12.027.

[13] J. Stoll, N. Zhao, X.-Z. Yuan, F. Girard, E. Kjeang, Z. Shi, Impacts of cathode catalyst layer defects on performance and durability in PEM fuel cells, J. Power Sources 583 (2023) 233565, https://doi.org/10.1016/j.jpowsour.2023.233565.

[14] H. Liu, L. Ney, N. Zamel, X. Li, Effect of catalyst ink and formation process on the multiscale structure of catalyst layers in PEM fuel cells, Appl. Sci. 12 (2022) 3776, https://doi.org/10.3390/app12083776.

[15] J. Zhao, X. Li, Z. Liu, The effect of ink dilution and evaporation on the microstructures of catalyst layers in polymer electrolyte membrane fuel cells, Int. J. Energy Res. (2019) er.4671, https://doi.org/10.1002/er.4671.

[16] C.-Y. Ahn, S. Jang, Y.-H. Cho, J. Choi, S. Kim, S.M. Kim, et al., Guided cracking of electrodes by stretching prism-patterned membrane electrode assemblies for high-performance fuel cells, Sci. Rep. 8 (2018) 1257, https://doi.org/10.1038/s41598-018-19861-6.

[17] S.M. Kim, C.-Y. Ahn, Y.-H. Cho, S. Kim, W. Hwang, S. Jang, et al., High-performance fuel cell with stretched catalyst-coated membrane: one-step formation of cracked electrode, Sci. Rep. 6 (2016) 26503, https://doi.org/10.1038/srep26503.

[18] G.W. Scherer, Theory of drying, J. Am. Ceram. Soc. 73 (1990) 3–14, https://doi.org/10.1111/j.1151-2916.1990.tb05082.x.

[19] A.F. Routh, Drying of thin colloidal films, Rep. Prog. Phys. 76 (2013) 046603, https://doi.org/10.1088/0034-4885/76/4/046603.

[20] K.B. Singh, M.S. Tirumkudulu, Cracking in drying colloidal films, Phys. Rev. Lett. 98 (2007) 218302, https://doi.org/10.1103/PhysRevLett.98.218302.

[21] M.S. Tirumkudulu, W.B. Russel, Cracking in drying latex films, Langmuir 21 (2005) 4938–4948, https://doi.org/10.1021/la048298k.

[22] P. Quarz, N. Zimmerer, P. Scharfer, W. Schabel, About drying phenomena of fuel cell and electrolyzer CCM inks: Selectivity of the evaporation of 1-propanol/water mixtures, Fuel Cells (2024) fuce.202300252, https://doi.org/10.1002/fuce.202300252.

[23] T. Riede, E.U. Schlünder, Evaporation and pervaporation of a binary mixture from an inert carrier liquid, Chem. Eng. Technol. 11 (1988) 384–391, https://doi.org/10.1002/ceat.270110150.

[24] M. Koga, H. Matsumoto, M. Tokita, H. Masunaga, T. Hikima, H. Sugimori, et al., Investigation of drying process of catalyst ink for polymer electrolyte fuel cells by grazing-incidence X-ray scattering, ECS Trans. 86 (2018) 157–161, https://doi.org/10.1149/08613.0157ecst.

[25] F. Thurner, E.U. Schlünder, Wet-bulb temperature of binary mixtures, Chem. Eng. Process. Process. Intensif. 19 (1985) 337–343, https://doi.org/10.1016/0255-2701(85)85006-6.

[26] P. Quarz, N. Zimmerer, L. Janning, A.-M. Steck, P. Scharfer, W. Schabel, Ink processing and its influence on particle size distribution, ionomer requirements and electrode properties in polymer electrolyte membrane fuel cell and electrolyser catalyst coated membranes, Energy Tech. (2025), https://doi.org/10.1002/ente.202501844.

[27] T. Van Cleve, S. Khandavalli, A. Chowdhury, S. Medina, S. Pylypenko, M. Wang, et al., Dictating Pt-based electrocatalyst performance in polymer electrolyte fuel cells, from formulation to application, ACS Appl. Mater. Interfaces 11 (2019) 46953–46964, https://doi.org/10.1021/acsami.9b17614.

[28] T.T. Ngo, T.L. Yu, H.-L. Lin, Influence of the composition of isopropyl alcohol/water mixture solvents in catalyst ink solutions on proton exchange membrane fuel cell performance, J. Power Sources 225 (2013) 293–303, https://doi.org/10.1016/j.jpowsour.2012.10.055.

[29] C.M. Baez-Cotto, J.R. Pfeilsticker, H. Yu, T. Van Cleve, B.T. De Villers, C. F. Cetinbas, et al., Impact of polymer additives on crack mitigation of rod-coated fuel cell cathode catalyst layers, J. Power Sources 592 (2024) 233852, https://doi.org/10.1016/j.jpowsour.2023.233852.

[30] M. Léang, F. Giorgiutti-Dauphiné, L.-T. Lee, L. Pauchard, Crack opening: from colloidal systems to paintings, Soft Matter 13 (2017) 5802–5808, https://doi.org/10.1039/C7SM00985B.

[31] D.-C. Huang, P.-J. Yu, F.-J. Liu, S.-L. Huang, K.-L. Hsueh, Y.-C. Chen, et al., Effect of dispersion solvent in catalyst ink on proton exchange membrane fuel cell performance, Int. J. Electrochem. Sci. 6 (2011) 2551–2565, https://doi.org/10.1016/S1452-3981(23)18202-2.

[32] N. Zimmerer, P. Quarz, E. Terhorst, L. Janning, P. Scharfer, W. Schabel, Influence of ink formulation and drying parameters on component composition during drying of catalyst layers for polymer electrolyte membrane (PEM) fuel cells and electrolyzers, Energy Technol. (2025), https://doi.org/10.1002/ente.202500516.

[33] S. Jaiser, M. Müller, M. Baunach, W. Bauer, P. Scharfer, W. Schabel, Investigation of film solidification and binder migration during drying of Li-Ion battery anodes, J. Power Sources 318 (2016) 210–219, https://doi.org/10.1016/j.jpowsour.2016.04.018.

[34] S. Jaiser, A. Friske, M. Baunach, P. Scharfer, W. Schabel, Development of a three-stage drying profile based on characteristic drying stages for lithium-ion battery anodes, Dry. Technol. 35 (2017) 1266–1275, https://doi.org/10.1080/07373937.2016.1248975.

[35] A. Altvater, J. Klemens, J. Borho, A. Smith, T. Heckmann, P. Scharfer, et al., Application of multistage drying profiles for accelerated production of Li-ion battery anodes using infrared radiation: validation with electrochemical performance and structural properties, Energy Tech. 12 (2024), https://doi.org/10.1002/ente.202301272.

[36] VDI e. V, VDI-Wärmeatlas (editor), Springer Berlin Heidelberg, Berlin, Heidelberg, 2013, https://doi.org/10.1007/978-3-642-19981-3.

[37] Peng D.-Y. Extending the Van Laar Model to Multicomponent Systems n.d.

[38] S. Takahashi, T. Mashio, N. Horibe, K. Akizuki, A. Ohma, Analysis of the microstructure formation process and its influence on the performance of polymer electrolyte fuel-cell catalyst layers, ChemElectroChem 2 (2015) 1560–1567, https://doi.org/10.1002/celc.201500131.

[39] Atkinson A., Guppy R.M. Mechanical stability of sol gel films, 1991.

[40] J. Park, Z. Kang, G. Bender, M. Ulsh, S.A. Mauger, Roll-to-roll production of catalyst coated membranes for low-temperature electrolyzers, J. Power Sources 479 (2020) 228819, https://doi.org/10.1016/j.jpowsour.2020.228819.